UNIVERSITY OF CALIFORNIA
RIVERSIDE

Fabrication and Capillary Flow in Microporous Aluminum Nitride for Non-Thermal Solar Desalination

A Thesis submitted in partial satisfaction
of the requirements for the degree of

Master of Science

in

Mechanical Engineering

by

James Li-Guo Leung

December 2022

Thesis Committee:
Dr. Luat Vuong, Chairperson
Dr. Bhargav Rallabandi
Dr. Kambiz Vafai

The Thesis of James Li-Guo Leung is approved:

Committee Chairperson

University of California, Riverside

ABSTRACT OF THE THESIS

Fabrication and Capillary Flow in Microporous Aluminum Nitride for Non-Thermal Solar Desalination

by

James Li-Guo Leung

Master of Science, Graduate Program in Mechanical Engineering
University of California, Riverside, December 2022
Dr. Luat Vuong, Chairperson

Aluminum Nitride (Al-N) is a white, hydrophilic, thermally-conducting, high-band-gap ceramic with low visible-light-spectrum emissivity. Aluminum Nitride being hydrophilic makes it capable of utilizing capillary action, which means it can be used as a material for wicking.

Here we report on the light-induced evaporation of saltwater through a capillary wick composed of drop-cast, loosely bonded Al-N microparticles. With 405-nm LED light illuminating the wick, water evaporation rates are increased to levels above equivalent-energy thermal evaporation rates. We checked for the effect of humidity and crystallization on the trials, and showed how both act as inevitable inhibitors to the evaporation process. Oscillations in the evaporation rate occur as well, caused by a dominance in either crystallization or dissolution in the pores. Our observations point to the potential of a novel solar non-thermal desalination approach.

TABLE OF CONTENTS

LIST OF FIGURES

Introduction

Desalination

Solar-thermal desalination processes involve the conversion of absorbed light into heat, which evaporates and separates water from a saltwater reservoir. These processes cannot achieve 100 percent efficiency though, as inefficiency arises from any heat leakage from the solar desalinating mechanism to its surroundings such as the bulk reservoir, where water's high specific heat capacity allows the bulk reservoir to maintain a lower temperature. [1][2] Heat leakage occurs from the entropy-driven transfer processes such as: thermal diffusion, photon thermalization of black-body emission, or the heat released when vapor condensation. Additionally, there are inevitable losses due to conduction and convection from the water in contact with the substrate and/or reservoir. Thermal radiation of the captured heat must also be mitigated. [2] This thermal emittance is significant with solar thermal concentration designs, since radiative heat losses scale with the fourth power of the surface temperature.

These inevitable leakages of the already-captured heat are not the only unavoidable challenges to contend with in the thermal desalination paradigm. The water-to-steam conversion is an energy-intensive process simply due to the high latent heat of vaporization of water. This means more energy goes into changing the phase of the liquid water.

It is important to mention that in spite of the challenges, researchers have achieved ways of mitigating the inefficiency by recycling the energy from the condensation process and by designing the spectral properties of windows and surfaces. Multistage processes reduce leakage with infrared-reflecting windows and surfaces that recapture the heat released from the vapor condensing have been demonstrated by Xu et al. This process is referred to as enthalpy recycling. [1][2][3]

Knowledge of interfacial thermal and radiative processes will also enable new solar desalination and zero-liquid discharge technologies. Solar-thermal desalination involves three important subprocesses, which are described: (i) thermal conversion and transport; (ii) ion transport and salt dissipation; (iii) vapor manipulation and water yield. In general, interfacial solar desalination systems require high evaporation temperatures and high vapor generation rates, which can be achieved by increasing the solar absorption and reducing the heat loss through conduction, convection, and radiation. [2][3][4]

Other keys to mitigating thermal leakage involve reducing the area of the water path to reduce the heat loss through conduction, increasing the distance of the heating location from the reservoir, or localizing the heating of the water into small packets at a time. While not seeking to utilize heat, the principles of mitigating potential energy loss and also packetizing the water will be utilized in our system. [3][4]

Capillary Action and Imbibition

Packetizing of liquid helps when we consider its benefits to evaporation. The Hertz–Knudsen (H–K) equation relates the evaporated mass flux from the surface of a liquid in relation to the pressure differences that develop in the liquid during evaporation. However, tests from Hoyst et al. have suggested that something more guides evaporation other than the pressure of the liquid and equilibrium pressure. Evaporation via capillary methods further drives this point home, as such methods seem to bypass predicted values as calculated by the H-K equation. [5]

Capillary action transports liquids without mechanical input. Because it typically happens through small channels, the process funnels the liquid into smaller units of water at a time. thus enabling more exposure of the liquid to air and thus more evaporation of the water. [6][7] Capillary action only occurs when the adhesive forces between a liquid and its surroundings are greater than the cohesive forces within itself, thus the wicking material must be more hydrophilic than water. This allows a liquid to pull itself up through a narrow channel without the aid of external forces. In a porous material like a paper towel, each pore acts as a narrow channel in which capillary action takes effect; this is what's responsible for paper towels' ability to pick up water in a process called imbibition. The effect of imbibition then essentially packetizes the bulk water, increasing the overall surface area per unit volume of the liquid and consequently making vaporization occur more readily. [6]

Liquid molecules moving on or between interfaces experience larger free energy gradients than those escaping from the middle of bulk liquid or pore channels. Liquid near the solid surface tends to form into monolayers, which leads to a high potential energy in the liquid. [6] There is a smaller energy barrier between the liquid and vapor phases of water where the liquid comes into contact with the walls of the solid. Thus, evaporation of the liquid increases near the interfaces. [7]

The inspiration for this stems from the studying of plants, particularly mangroves. Mangroves grow in intertidal zones, where the sea meets rivers and other similar fresh water sources. This means they must be able to filter the salt water they absorb in order to live, which is done via forcing the salt water through a semipermeable membrane and then forcing the remaining salt out of pores in their leaves. The leaves are also the location where evaporation occurs; this evaporation is also key, as it generates negative pressure zones in the plant's capillaries which aids the plant's filtration mechanism. [8]

Our system will use aluminum nitride microparticles sintered together to act as the porous material in which capillary action can be utilized, the packed particles become analogous to a porous medium. The packed microparticles should not be so large that they do not form capillaries, but not so small that they themselves impede the movement of the water molecules. While we will be using the same idea of capillary action and evaporation driven water dynamics, we will not be using a filter for salt. Instead, we hope to utilize a phenomenon called salt creep for further separation of the salt and water.

Salt Crystallization and Salt Creep

When a solute dissolves in a solvent, the solvent molecules surround the solute molecules and pull them apart. In this case, sodium chloride molecules are torn into sodium cations and chloride anions by the strong polar properties of the solvent, water. Once these ions are formed in the solution, they soon "coordinate" the water into forming a network of bonds in the solvent-solute that act like a mesh that holds the ions within it. While solvents have solutes dissolved into them, a number of their physical and chemical properties are affected. [9] [10]

Le et al.'s paper suggests that the location of salt crystallization also depends on the ratio of water evaporation from the pores to the supply of water to the pores from capillary action. Crystallization will occur deeper in the pores when the evaporation rate exceeds the water supply rate, a result that as mentioned previously should be avoided in order to prevent salting out. This crystallization begins in zones of supersaturation, located around the vapor-liquid interface of the meniscus and depositing on the liquid-solid interface. [11]

Salt creep also occurs on the wick as the evaporation proceeds. The salt crystallizes wherever the liquid/air interface is, namely the meniscus formed by the liquid in the pores. This does cause the salt to crystallize both inside and outside the pores of the wick though primarily on the outside surfaces; whenever the meniscus does drop deeper into the pores, salt will start nucleating inside the channels. [12]

The salt that crystallizes onto the wick either helps or hinder the evaporation process depending on the location of crystallization. Salt in a solution serves to decrease the vapor pressure of the solution, because the mere presence of the salt solute decreases the amount of the water solvent spots on the surface of the liquid to evaporate. The salt that crystallizes onto/inside the pores themselves does clog it and thus hinders the fluid transport in the capillary. [13] On the other hand, salt that crystallizes on the outer edges of the porous material sample leads to growth of larger crystals, because the new salt crystals serve as new areas for the salt solution to nucleate. The movement of the salt solution does get transported to the crystallization edge as well, serving as another platform for liquid water transfer. [12]

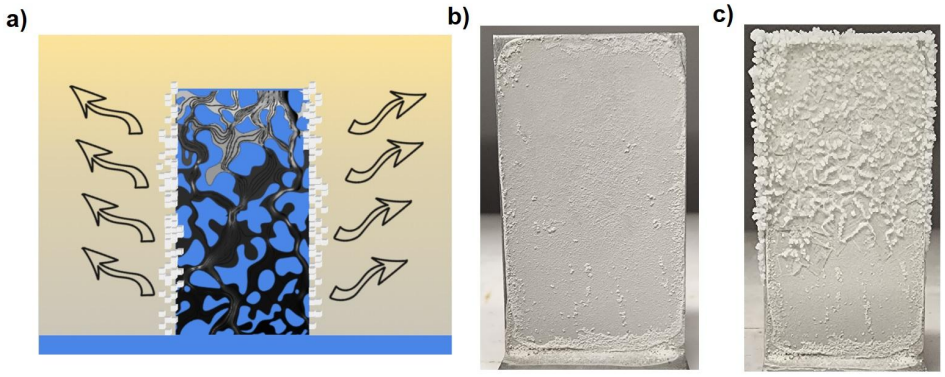

Figure 1: a) Depiction of the expected processes of both salt crystallization and water evaporation as water is wicked up into the aluminum nitride micropores b) Aluminum nitride wick pre-trial c) Aluminum nitride wick post-trial with 300000 ppm salinity water

This research focuses on light-induced potentials that combine with capillary-based desalination processes that bypass the need for heat. We utilize capillary action, water packetizing, reduction of free-energy barrier from interfacing of solid-liquid-vapor, salt crystallization creep, and non-thermal solar energy input.

Experimental Section

Wick Fabrication

We fabricated our porous, aluminum nitride (Al-N) wicking material via repeated drop-casting of a solution of aluminum nitride microparticles and deionized water onto a heated Alloy-3003 aluminum substrate. The aluminum nitride particles are 10 microns large at a 99% consistency. The slurry solution consists of ~ 0.25 g of Al-N to ~30 mL of water and, as Al-N is not water soluble, requires constant stirring by hand.

The substrate gets heated on a hot plate up to 100 C initially; any higher temperature triggers the Leidenfrost effect and therefore makes the solution incapable of depositing onto the aluminum substrate. Then the slurry solution is swirled thoroughly to generate a rough emulsion, as Al-N and water do not mix well, before a layer is then applied on to the aluminum by “dragging” the solution across the surface to create a film. Once a layer is deposited, the heat is brought up to 200 C to dry and then brought back down to 100 C again to avoid the Leidenfrost effect. These steps are repeated until no more slurry solution is available.

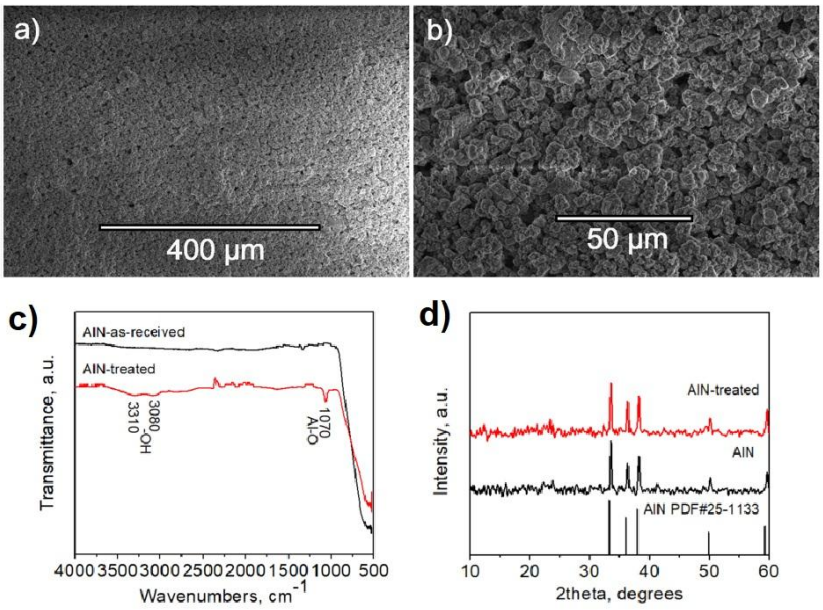

Figure 2: a) Pre-trial at 400 µm relative size b) Pre-trial at 50 µm relative size c) FTIR comparison of Al-N before and after deposition process on wick d) XRD analysis of Al-N before and after deposition process on wick

After the fabrication of a sample, the wicking layer was brought to a TESCAN VEGA3 SEM machine to capture SEM images, depicting the microparticles to check for any phase changes. Figure 2 a) and b) shows how the Al-N particles are loosely bonded to each other, with multiple pores/channels of roughly the same diameter as the particles themselves. Then a sample portion of the wicking layer was taken along with the original Al-N microparticles to be analyzed with Fourier-Transform Infrared (FTIR) and X-Ray Diffraction (XRD) Spectroscopy machines. Figure 2 c) and d) are the FTIR and XRD analysis showing any changes the Al-N might have undergone during the deposition process. The FTIR shows that the treated sample contains slight amounts of -OH groups, indicating the formation of Al(OH)3. The treated sample has some quantities of

nano-sheet structures on the surface, in this case it is the typical structure of Al(OH)3 which the presence of is previously confirmed in the FTIR. The XRD shows that the treated sample is still primarily Al-N, and no fundamental changes occurred during the fabrication process.

Experimental Setup

Experiments were done in a sealed, acrylic glove-box that has dimensions of 24 x 36 x 18 inches. A tarp covers the box to both protect from LED glare and also minimize light interference. Humidity levels were brought down to initial conditions using silicon-gel desiccants; desiccant was taken out once trials started, so humidity inside the box was not controlled throughout the trials. The optical setup starts from a 405 nm LED that is focused down with a lens into an aperture. This controls the amount of light going into a collimating lens that re-columnizes the light before it goes into a cylindrical lens, which changes the shape of the beam into an elliptical shape. The cylindrical lens is held on an octagonal holder that we designed and 3D printed. This allows us to change the orientation of the light into either vertical or horizontal orientations. The beam has an approximate area of 1 cm^2. We achieve intensities of ~150 mW/cm^2 that reach the wick from this setup. Compared to the average solar illumination on the Earth's surface of 100 mW/cm^2, that means we are using about 1.5 times the average solar illumination.

We shined the 405 nm LED light onto the porous wick made of drop-coated 10 um Aluminum Nitride particles. Mass measurements were taken on an Ohaus™

Explorer™ micro-balance, at intervals of every minute for a total of 900 minutes. Relative humidity, temperature, and pressure were measured on a Fisherbrand™ Traceable™ Excursion-Trac™ USB Datalogging barometer, where data points were also taken every minute. The incident light power was measured using a Thorlabs™ S310C - Thermal Power Sensor Head. The trials used a salt solution of salinity 300,000 ppm in order to mimic waste brine salinity. Mass rate data was taken by taking the initial mass and subtracting subsequent weight data minute by minute.

Results

The mass rate data, henceforth called evaporation rate, was processed in Python using the sav.gol filter function from scipy library, with a window length of 21 points, a polynomial order of 2, and in 'interp' mode, in order to smooth out noise. The evaporation rate comparison between the first vertical and horizontal orientation trials showed a similar magnitude of performance, with no discernible differences that could not be attributed to noise. The second trials of each had differing humidities. This led to the rest of the experiments being done with horizontally-oriented light.

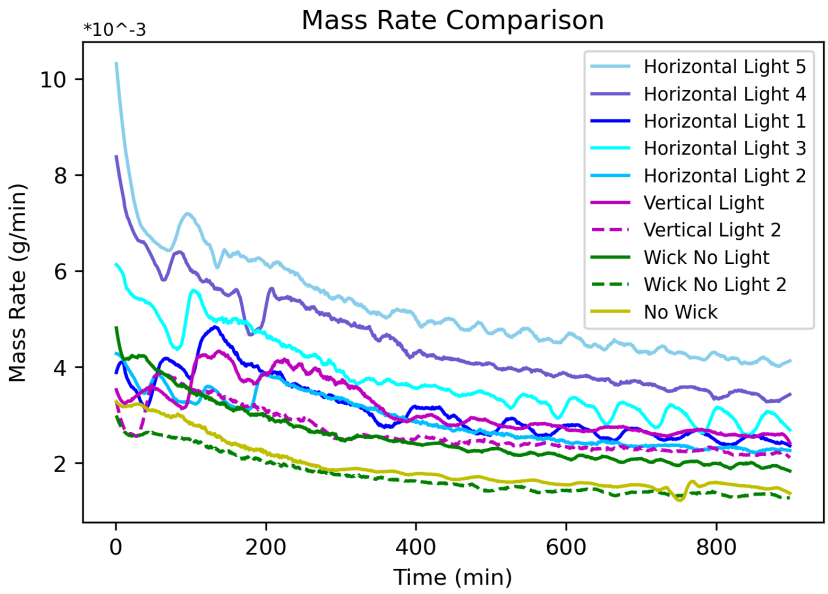

Figure 3: A comparison of the different calculated mass rates that each trial achieved under different conditions.

The evaporation rate without wick is lower than all trials with wick, and further increases with the presence of light, as seen in Figure 3. This means the aluminum nitride wick effectively shows an ability to increase the evaporation rate of water under illumination. Using an illumination of 150 mW over 1 cm^2 area, about 1.5 suns, we achieved rates of: 1.57, 1.86, 2.25, 2.70, and 3.13 kg m^{-2} hr^{-1} using the horizontal orientation of light at decreasing levels of starting relative humidity.

The evaporation flux at 55% starting relative humidity. 1.57 kg m^{-2} hr^{-1}, is within the same magnitude as other evaporation experiments that mainly focus on solar-thermal conversions and black surfaces. For example, in 2015 Ito et al. developed doped (N) and undoped (G) porous graphene sheets grown at different temperatures (800 C, 950C). Under an intensity of about 1 sun, they were capable of 1.5 kg m^{-2} hr^{-1} for N950, 1.32 kg

m^{-2} hr^{-1} for G950, 1.14 kg m^{-2} hr^{-1} for N800, and 1.04 kg m^{-2} hr^{-1} for G800. [14] In 2020, Singh et al. utilized laser treatments to convert an aluminum sheet into a SWSA (super-wicking super-light-absorbing) surface, a black panel with microchannels that achieved evaporation rates under an intensity of 1 sun of kg m^{-2} hr^{-1} and 0.5 kg m^{-2} hr^{-1} for double-sided and single-sided sheets respectively. [15]

Heat vs. Light Effects

We ran calculations for the amount of light energy absorbed by the system as well as the amount of thermal energy required to boil the same amount of water that our system evaporated. This was to check if the observed evaporation rates are indeed photomechanical, non-thermal dynamics and not thermal-based on light shining.

Due to our wicking Al-N layer consisting of roughly drop-casted circular microparticles, we estimate an average incident angle of 0 degrees. We then calculate the reflection and transmission coefficient of our Al-N films using Fresnel's equations, this average incident angle, and refractive index values found by Joo et al, Khoshman et al and Alsaad et al. [16][17][18] The reflection and transmission come out to be at approximately 0.15 and 0.75. With Al-N having approximately 0.15 reflectance and 0.75 transmittance, its absorbance would be at 0.1.

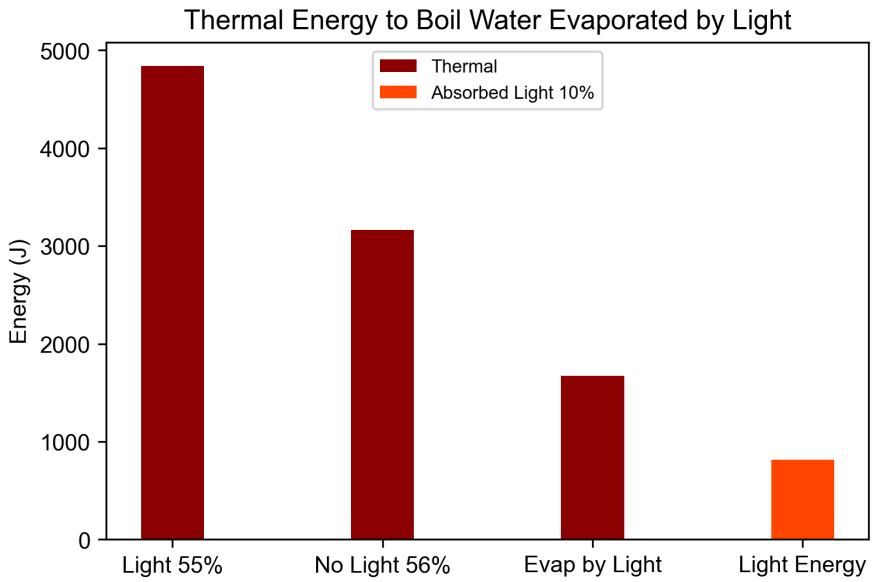

Figure 4: A comparison of the required energy to thermally boil an amount of liquid for varying starting relative humidities vs. how much light energy was absorbed by the system. With Al-N having approximately 0.15 reflectance and 0.75 transmittance, its absorbance would be at 0.1; we thus assume 10% of the light is absorbed by the wick.

We calculated the thermal energy that would be used to evaporate each amount of water to be and compared it to the expected amount of light energy absorbed by the wick system. First, we find the boiling point elevation using the boiling point elevation equation ΔT = Kib. [21][22]

Equations:

$$\Delta T_{Boil} = Kib \tag{1}$$

$$Q = C_{solution}(m_{water} + m_{salt})(T_0 + \Delta T_{Boil} - T_i) \tag{2}$$

Equation (1) gives the boiling point temperature elevation of water when a solute is dissolved into it. $\boldsymbol{K}$ is the Ebullioscopic constant (units K kg/mol) which relates molality to boiling point elevation, $\boldsymbol{i}$ is the van't Hoff factor which gives the number of particles the solute splits into when dissolved, and $\boldsymbol{b}$ is the molality of the solution.

We used equation Equation (2) to calculate how much energy it would have taken a thermal boiler to evaporate the same amount of water as our solar wick. We found an approximate value for the specific heat of the solution, $\boldsymbol{C_{solution}}$, via extrapolation of the data found in Randall et al's experiments.[23] We do the same with data from Sharqawy et al's data for the latent heat of vaporization of the solution.[24]

The energy comparison between an estimated thermal boil and our solar desalination wick system in Figure 5 shows that our method does not primarily use thermal methods to evaporate water. Heating the system is unavoidable while the system is under illumination, but this comparison serves to separate our desalination method from other projects, which utilize solar-to-thermal converters. Further study will be required to pinpoint the exact effect of light.

Humidity Effect

We define relative humidity (RH) as the amount of water vapor in the air versus the amount of water vapor the air can hold at saturation, but it can also be described as the ratio of water vapor pressure to the water vapor saturation pressure.

We can get an idea for this change in vapor pressure from the equation for vapor pressure of solution from Raoult's Law: $P_{solvent} = X_{solvent} P_{solvent}$ where $P_{solvent}$ is the vapor pressure of the solvent above the solution, $X_{solvent}$ is the mole fraction of the solvent in the solution, and $P_{solvent}$ is the vapor pressure of the pure solvent.

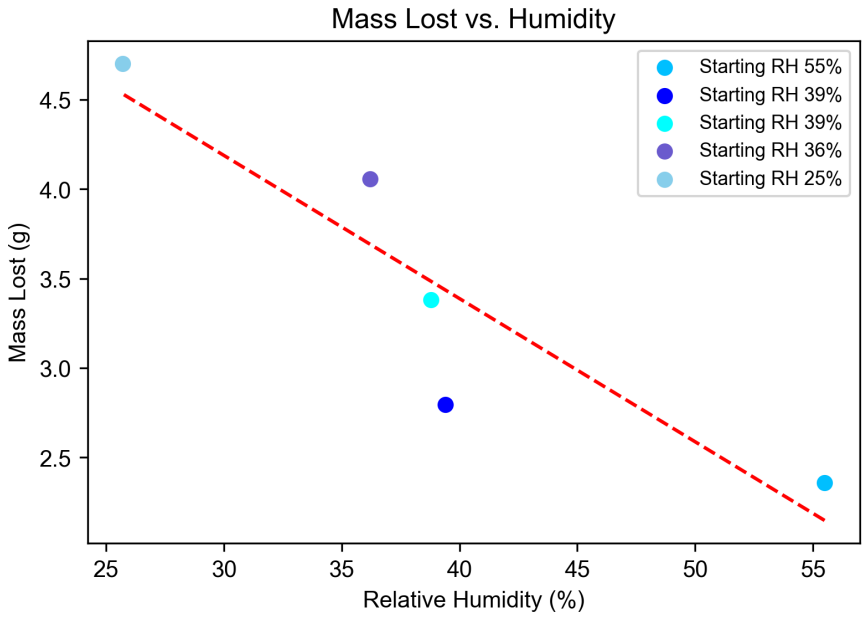

Figure 5: A depiction of the effect that increasing starting relative humidity (and consequently increased overall humidity over the trial) leads to lower evaporation.

The steady overall decline in the entire trial's evaporation across different trials coincides with increase in humidity inside the experimental system. Increases in humidity raise the free energy barrier for water to evaporate until it reaches an equilibrium.

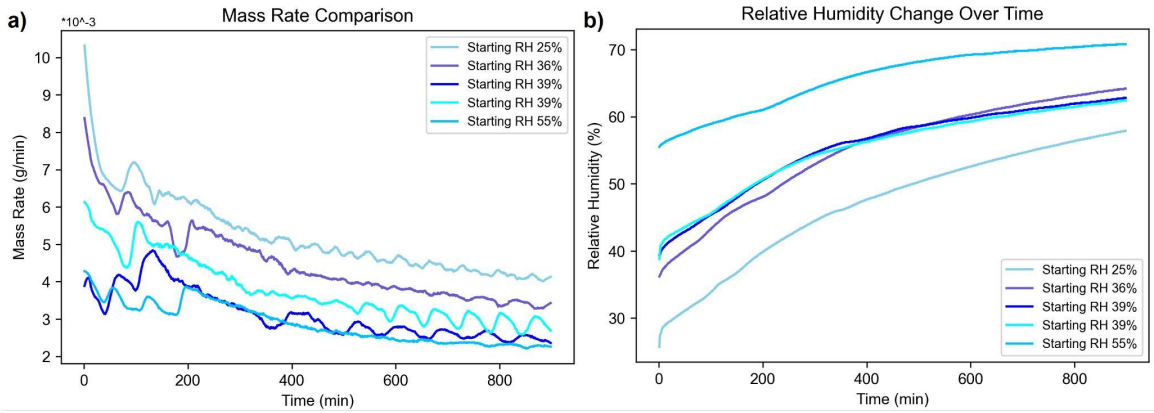

Figure 6: a) A chart of the evaporation rates done with different starting relative humidities b) A chart of the change in relative humidity over the course of the same trials. The charts seem to follow the inverse trend of each other.

The RH of the volume increases over time as the wick evaporates water. The humidity increase over time follows a logarithmic growth, while the evaporation rate trend does the inverse, showing that an increase in RH in the system coincides with a decrease in the evaporation rate. Rising humidity increases the vapor pressure required for water to evaporate, in other words, it increases the energy barrier in the system for evaporation, which makes it more difficult for water to evaporate.[25]

Hamdan et al. checked for weight loss percentage, so a difference between 22%RH and 85%RH (+63%) led to a difference of ~8% weight loss.[25] In our experiments, the %RH change is from 36%RH to 55%RH (+19%), leading to a difference of weight loss percentage equal to 13.5% and 11.1% respectively, a difference of ~ 2.4% weight loss. This leads to a ratio of 3.31 and 3.33 between %RH and weight loss difference, which may indicate a linearly proportional relationship between humidity and evaporation performance at these levels of humidity.

This humidity-controlled effect can be assumed to be negligible in an open environment, even though it still occurs, because the evaporated water will diffuse away from the system due to exposure to the environment; we placed the wick in a closed system, isolated from the environment in order to mitigate the effect of potential variables such as wind/air flow, and temperature changes in order to study this effect.

Salt Crystallization and Salt Creep Effect

Initial nucleation of salt crystals depends on the localized surface concentration of sodium and chloride ions, which is controlled by the location of evaporation fluxes at the surface.[26][27][28][29] We expect greater evaporation fluxes to occur near the periphery of the wick, due to the higher number of solid-liquid-vapor interfaces near the edges.[30][31][32] This effect can be seen in Figure 8, where the edges of the wicks have visually larger crystals of salt than those on the surface. Unfortunately, quantifying this effect can be difficult even with molecular dynamic simulations, as the very nature of porous materials are disordered tunnels at a micro- and lower scale.

Not only that, there are two separate types of disorders present in these porous materials: surface and internal disorders. Surface disorders determine the variations in evaporation rates across the surface of the wick while internal disorders determine the variations in sodium/chloride concentrations within the salt solutions being wicked up. These disorders are random, and consequently the locations for nucleation and subsequent crystallization are randomized as well.[33]

The resulting salt formations after our trials follow the expected patterns, where it appears to preferentially crystallize around edges and/or forming clusters on the face of the wick, presumably the initial nucleation points on the face. This indicates solid-liquid-air interface-based and also nucleation-location based crystallization. When evaporation happens rapidly in the beginning, salt starts nucleating closer to the bottom of the wick (the beginning of the waterfront); when it is slower, more of the wick becomes imbibed and thus more sporadic but spread-out nucleation occurs.

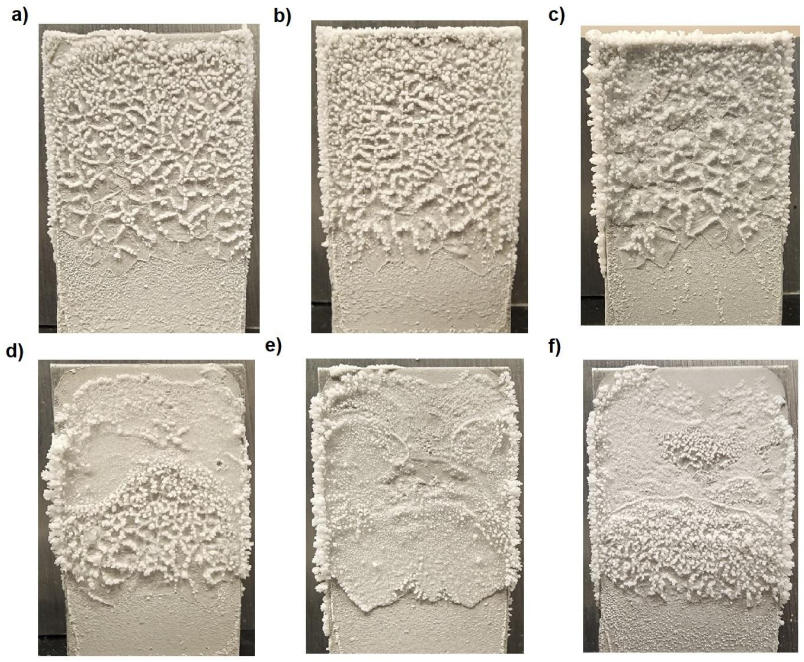

Figure 7: A comparison of the different salt crystallization patterns across different trials at different humidities. a) No light with starting RH 56% b) Light with starting RH 55% c) Light with starting RH 39% d) Light with starting RH 39% e) Light with starting RH 36% f) Light with starting RH 26%

The crystallization patterns also show signs of salt creep, as salt crystals not only branch outward from the edges of the wick, particularly in Figure 8 c), d), e), and f) which uncoincidentally have the higher evaporation rates. The salt growth in those particular trials also branched onto the sides of the wick (not visible in Figure 8). [12]

Figures 7 and 8 show that the evaporation of the wick slows but does not stop, even with full coverage of the wick face by salt crystallization over the 15 hour trial. The salt crystals instead appear to take over some parts of the capillary action from the Al-N, though at a much slower rate starting from 400 minutes into the trial. There is a distinct possibility that the slopes level out when salt covers the face of the wick, as salt crystals reflect much more light and thus diminishes the contribution of light. Still, this result indicates that our wick can be utilized for self-actuated salt-creep and thus salt removal from a reservoir.

Evaporation Rate Oscillations

Some of the experiments showed a pattern developing near the latter half of their run in which the evaporation rate would increase and decrease periodically in an oscillatory pattern, viewable in Figure 7 a). This phenomenon can be very readily seen in the runs with starting RH 39%. We believe these oscillations in evaporation rate could stem from cycles of evaporation and crystallization, into dissolution, and back to evaporation. The decrease in evaporation rate stems from the blockage of pores from the interior formation of salt crystals coupled with a hindrance of light absorption from the

exterior salt crystallization.[13] The upswing after this decline comes from the salt gradient that develops during the process; the localized salt concentration in the pores and the surface are higher than at the reservoir due to evaporation and thus induces some water movement.[30][31][32] The interior pores clogged by the salt crystals are re-hydrated and some water climbs up onto the exterior crystals, dissolving the interior salt crystals back into a solution while the exterior crystals remain in place but undergo salt creep.[12][33] These cyclic processes then repeat through till the end experiment.

Both crystallization and dissolution are happening simultaneously, but whichever rate is higher determines the slope direction. Downward slopes are driven by evaporation leaving behind salt crystals that: if formed on the surface, start reflecting more light; if formed deeper in pores, impedes water movement.[13][34] Upward slopes start when dissolution overtakes, reopening some pathways.[26][33] Larger crystals that formed on the surface are capable of transferring water over their surface as well, so they begin growing and/or creeping.[12]

Light and humidity affect the oscillations as well. Oscillations still occur in trials without light, but light seems to both enhance the amplitude and increase the length of the upward and downward slopes of the oscillations. Higher humidities meanwhile have dampened amplitudes. These experiments are nonlinear systems though, so initial conditions affect the process of the evaporation as well as the crystallization. Thus, precise reasons for the oscillations as well as any conditions that affect them need further study.

Conclusion

We have shown that our thin, microporous-layer of aluminum nitride is capable of evaporation of high salinity brines under 405 nm light, with evaporation rates between 1.57 and 3.13 kg m^{-2} hr^{-1} depending on the relative humidity of the surroundings. Higher relative humidity meant lower overall evaporation. The system does this non-thermally, but the actual effect that light has on the system will be a future study topic. The working theory is that it increases the free energy of the system in order to enhance evaporation. Oscillations also occur in the latter half of some of the experiments. They may be stemming from a cycle of evaporation, crystallization, dissolution and salt creep. This evaporation method acts as a nonlinear system, so initial conditions greatly affect the process. Precise actuators/catalysts require further study as well.

The wick can be utilized for salt creep and cleaning of high salinity brines. Brine generated from factories and other water-purification processes harms the environment; if instead the salt and water in brine were separated by crystallizing the salt and/or evaporating the liquid water, the solid by-products are easier and safer to dispose of.

In addition to that, Al-N in this form acts like a white surface with low visible-light-spectrum emissivity that emits in the infrared atmospheric window. This means our wick can possibly be used as a radiative cooling system, keeping the average surface temperature of the location lower than its surroundings during the day, and colder still at night. If fine-tuned and well-designed, a system utilizing this method can avoid environmental damages that arise from thermal methods of evaporation.

Bibliography

[1] Liu, G., Chen, T., Xu, J., Yao, G., Xie, J., Cheng, Y., Miao, Z., & Wang, K. (2021). Salt-Rejecting Solar Interfacial Evaporation. In Cell Reports Physical Science (Vol. 2, Issue 1, p. 100310). Elsevier BV. https://doi.org/10.1016/j.xcrp.2020.100310

[2] Wang, Z., Horseman, T., Straub, A. P., Yip, N. Y., Li, D., Elimelech, M., & Lin, S. (2019). Pathways and challenges for efficient solar-thermal desalination. In Science Advances (Vol. 5, Issue 7). American Association for the Advancement of Science (AAAS). https://doi.org/10.1126/sciadv.aax0763

[3] Xu, Z., Zhang, L., Zhao, L., Li, B., Bhatia, B., Wang, C., Wilke, K. L., Song, Y., Labban, O., Lienhard, J. H., Wang, R., & Wang, E. N. (2020). Ultrahigh-efficiency desalination via a thermally-localized multistage solar still. In Energy & Environmental Science (Vol. 13, Issue 3, pp. 830–839). Royal Society of Chemistry (RSC). https://doi.org/10.1039/c9ee04122b

[4] Liu, H., Huang, Z., Liu, K., Hu, X., & Zhou, J. (2019). Interfacial Solar‐to‐Heat Conversion for Desalination. In Advanced Energy Materials (Vol. 9, Issue 21, p. 1900310). Wiley. https://doi.org/10.1002/aenm.201900310

[5] Hołyst, R., Litniewski, M., & Jakubczyk, D. (2015). A molecular dynamics test of the Hertz–Knudsen equation for evaporating liquids. In Soft Matter (Vol. 11, Issue 36, pp. 7201–7206). Royal Society of Chemistry (RSC). https://doi.org/10.1039/c5sm01508a

[6] Fan, J., Wu, H., Wang, F., Evaporation-driven liquid flow through nanochannels. (2020). In Physics of Fluids (Vol. 32, Issue 1, p. 012001). AIP Publishing. https://doi.org/10.1063/1.5137803

[7] Vincent, O., Szenicer, A., & Stroock, A. D. (2016). Capillarity-driven flows at the continuum limit. In Soft Matter (Vol. 12, Issue 31, pp. 6656–6661). Royal Society of Chemistry (RSC). https://doi.org/10.1039/c6sm00733c

[8] Wang, Y., Lee, J., Werber, J. R., & Elimelech, M. (2020). Capillary-driven desalination in a synthetic mangrove. In Science Advances (Vol. 6, Issue 8). American Association for the Advancement of Science (AAAS). https://doi.org/10.1126/sciadv.aax5253

[9] Lyubartsev, A. P., & Laaksonen, A. (1996). Concentration Effects in Aqueous NaCl Solutions. A Molecular Dynamics Simulation. In The Journal of Physical Chemistry (Vol. 100, Issue 40, pp. 16410–16418). American Chemical Society (ACS). https://doi.org/10.1021/jp961317h

[10] Sheikholeslami, R. (2003). Nucleation and kinetics of mixed salts in scaling. In AIChE Journal (Vol. 49, Issue 1, pp. 194–202). Wiley. https://doi.org/10.1002/aic.690490117

[11] Le, D., Hoang, H., & Mahadevan, J. (2009). Impact of Capillary-Driven Liquid Films on Salt Crystallization. In Transport in Porous Media (Vol. 80, Issue 2, pp. 229–252). Springer Science and Business Media LLC. https://doi.org/10.1007/s11242-009-9353-x

[12] Qazi, M. J., Salim, H., Doorman, C. A. W., Jambon-Puillet, E., & Shahidzadeh, N. (2019). Salt creeping as a self-amplifying crystallization process. In Science Advances (Vol. 5, Issue 12). American Association for the Advancement of Science (AAAS). https://doi.org/10.1126/sciadv.aax1853

[13] Yang, Y., Zhao, H., Yin, Z., Zhao, J., Yin, X., Li, N., Yin, D., Li, Y., Lei, B., Du, Y., & Que, W. (2018). A general salt-resistant hydrophilic/hydrophobic nanoporous double layer design for efficient and stable solar water evaporation distillation. In Materials Horizons (Vol. 5, Issue 6, pp. 1143–1150). Royal Society of Chemistry (RSC). https://doi.org/10.1039/c8mh00386f

[14] Ito, Y., Tanabe, Y., Han, J., Fujita, T., Tanigaki, K., & Chen, M. (2015). Multifunctional Porous Graphene for High-Efficiency Steam Generation by Heat Localization. In Advanced Materials (Vol. 27, Issue 29, pp. 4302–4307). Wiley. https://doi.org/10.1002/adma.201501832

[15] Singh, S. C., ElKabbash, M., Li, Z., Li, X., Regmi, B., Madsen, M., Jalil, S. A., Zhan, Z., Zhang, J., & Guo, C. (2020). Solar-trackable super-wicking black metal panel for photothermal water sanitation. In Nature Sustainability (Vol. 3, Issue 11, pp. 938–946). Springer Science and Business Media LLC. https://doi.org/10.1038/s41893-020-0566-x

[16] Joo, H.-Y., Kim, H. J., Kim, S. J., & Kim, S. Y. (1999). Spectrophotometric analysis of aluminum nitride thin films. In Journal of Vacuum Science & Technology A: Vacuum, Surfaces, and Films (Vol. 17, Issue 3, pp. 862–870). American Vacuum Society. https://doi.org/10.1116/1.582035

[17] Khoshman, J. M., & Kordesch, M. E. (2005). Optical characterization of sputtered amorphous aluminum nitride thin films by spectroscopic ellipsometry. In Journal of Non-Crystalline Solids (Vol. 351, Issues 40–42, pp. 3334–3340). Elsevier BV. https://doi.org/10.1016/j.jnoncrysol.2005.08.009

[18] Alsaad, A. M., Al-Bataineh, Q. M., Qattan, I. A., Ahmad, A. A., Ababneh, A., Albataineh, Z., Aljarrah, I. A., & Telfah, A. (2020). Measurement and ab initio Investigation of Structural, Electronic, Optical, and Mechanical Properties of Sputtered Aluminum Nitride Thin Films. In Frontiers in Physics (Vol. 8). Frontiers Media SA. https://doi.org/10.3389/fphy.2020.00115

[19] Li, X., Liu, L., Zhao, J., & Tan, J. (2015). Optical Properties of Sodium Chloride Solution within the Spectral Range from 300 to 2500 nm at Room Temperature. In Applied Spectroscopy (Vol. 69, Issue 5, pp. 635–640). SAGE Publications. https://doi.org/10.1366/14-07769r

[20] Brown, M. E., Denman, W. T. P., & Trumbo, S. K. (2022). The Mid-UV Spectrum of Irradiated NaCl at Europa-like Conditions. In The Planetary Science Journal (Vol. 3, Issue 2, p. 28). American Astronomical Society. https://doi.org/10.3847/psj/ac457f

[21] Bialik, M., Sedin, P., & Theliander, H. (2008). Boiling Point Rise Calculations in Sodium Salt Solutions. In Industrial & Engineering Chemistry Research (Vol. 47, Issue 4, pp. 1283–1287). American Chemical Society (ACS). https://doi.org/10.1021/ie070564c

[22] Meranda, D., & Furter, W. F. (1977). Elevation of the boiling point of water by salts at saturation: data and correlation. In Journal of Chemical & Engineering Data (Vol. 22, Issue 3, pp. 315–317). American Chemical Society (ACS). https://doi.org/10.1021/je60074a023

[23] Randall, M., & Rossini, F. D. (1929). HEAT CAPACITIES IN AQUEOUS SALT SOLUTIONS. In Journal of the American Chemical Society (Vol. 51, Issue 2, pp. 323–345). American Chemical Society (ACS). https://doi.org/10.1021/ja01377a001

[24] Sharqawy, M. H., Lienhard, J. H., V., & Zubair, S. M. (2010). Thermophysical properties of seawater: a review of existing correlations and data. In Desalination and Water Treatment (Vol. 16, Issues 1–3, pp. 354–380). Informa UK Limited. https://doi.org/10.5004/dwt.2010.1079

[25] Hamdan, S., Ahmad, F. B. H., Dai, Y. Y., Dzulkefly, K., & Ku Bulat, K. H. (1999). EFFECT OF HUMIDITY ON EVAPORATION FROM AQUEOUS AND NONAQUEOUS MICROEMULSION WITH PERFUME. In Journal of Dispersion Science and Technology (Vol. 20, Issues 1–2, pp. 415–423). Informa UK Limited. https://doi.org/10.1080/01932699908943799

[26] Zimmermann, N. E. R., Vorselaars, B., Quigley, D., & Peters, B. (2015). Nucleation of NaCl from Aqueous Solution: Critical Sizes, Ion-Attachment Kinetics, and Rates. In Journal of the American Chemical Society (Vol. 137, Issue 41, pp. 13352–13361). American Chemical Society (ACS). https://doi.org/10.1021/jacs.5b08098

[27] Chakraborty, D., & Patey, G. N. (2013). How Crystals Nucleate and Grow in Aqueous NaCl Solution. In The Journal of Physical Chemistry Letters (Vol. 4, Issue 4, pp. 573–578). American Chemical Society (ACS). https://doi.org/10.1021/jz302065w

[28] Vekilov, P. G. (2005). Two-step mechanism for the nucleation of crystals from solution. In Journal of Crystal Growth (Vol. 275, Issues 1–2, pp. 65–76). Elsevier BV. https://doi.org/10.1016/j.jcrysgro.2004.10.068

[29] Lutsko, J. F., & Nicolis, G. (2006). Theoretical Evidence for a Dense Fluid Precursor to Crystallization. In Physical Review Letters (Vol. 96, Issue 4). American Physical Society (APS). https://doi.org/10.1103/physrevlett.96.046102

[30] Yang, Y., & Meng, S. (2007). Atomistic nature of NaCl nucleation at the solid-liquid interface. In The Journal of Chemical Physics (Vol. 126, Issue 4, p. 044708). AIP Publishing. https://doi.org/10.1063/1.2431363

[31] Tsai, J.-H., Perrotta, M. L., Gugliuzza, A., Macedonio, F., Giorno, L., Drioli, E., Tung, K.-L., & Tocci, E. (2018). Membrane-Assisted Crystallization: A Molecular View of NaCl Nucleation and Growth. In Applied Sciences (Vol. 8, Issue 11, p. 2145). MDPI AG. https://doi.org/10.3390/app8112145

[32] Le, D., Hoang, H., & Mahadevan, J. (2009). Impact of Capillary-Driven Liquid Films on Salt Crystallization. In Transport in Porous Media (Vol. 80, Issue 2, pp. 229–252). Springer Science and Business Media LLC. https://doi.org/10.1007/s11242-009-9353-x

[33] Veran-Tissoires, S., & Prat, M. (2014). Evaporation of a sodium chloride solution from a saturated porous medium with efflorescence formation. In Journal of Fluid Mechanics (Vol. 749, pp. 701–749). Cambridge University Press (CUP). https://doi.org/10.1017/jfm.2014.247

[34] Nooraiepour, M., Masoudi, M., Shokri, N., & Hellevang, H. (2021). Probabilistic Nucleation and Crystal Growth in Porous Medium: New Insights from Calcium Carbonate Precipitation on Primary and Secondary Substrates. In ACS Omega (Vol. 6, Issue 42, pp. 28072–28083). American Chemical Society (ACS). https://doi.org/10.1021/acsomega.1c04147

[35]
Li, J., Nam, K. B., Nakarmi, M. L., Lin, J. Y., Jiang, H. X., Carrier, P., & Wei, S.-H. (2003). Band structure and fundamental optical transitions in wurtzite AlN. In Applied Physics Letters (Vol. 83, Issue 25, pp. 5163–5165). AIP Publishing. https://doi.org/10.1063/1.1633965